Single-Atom Catalysis Hot Paper

How to cite: *Angew. Chem. Int. Ed.* **2021**, *60*, 21751–21755
International Edition: doi.org/10.1002/anie.202109488
German Edition: doi.org/10.1002/ange.202109488

Carbon Nitride Supported High-Loading Fe Single-Atom Catalyst for Activation of Peroxymonosulfate to Generate $^1O_2$ with 100 % Selectivity

Long-Shuai Zhang[+], Xun-Heng Jiang[+], Zi-Ai Zhong, Lei Tian, Qing Sun, Yi-Tao Cui, Xin Lu, Jian-Ping Zou, and Sheng-Lian Luo*

Abstract: *Singlet oxygen ($^1O_2$) is an excellent active species for the selective degradation of organic pollutions. However, it is difficult to achieve high efficiency and selectivity for the generation of $^1O_2$. In this work, we develop a graphitic carbon nitride supported Fe single-atoms catalyst (Fe_1/CN) containing highly uniform Fe-N_4 active sites with a high Fe loading of 11.2 wt %. The Fe_1/CN achieves generation of 100 % $^1O_2$ by activating peroxymonosulfate (PMS), which shows an ultra-high p-chlorophenol degradation efficiency. Density functional theory calculations results demonstrate that in contrast to Co and Ni single-atom sites, the Fe-N_4 sites in Fe_1/CN adsorb the terminal O of PMS, which can facilitate the oxidization of PMS to form $SO_5^{\bullet-}$, and thereafter efficiently generate $^1O_2$ with 100 % selectivity. In addition, the Fe_1/CN exhibits strong resistance to inorganic ions, natural organic matter, and pH value during the degradation of organic pollutants in the presence of PMS. This work develops a novel catalyst for the 100 % selective production of $^1O_2$ for highly selective and efficient degradation of pollutants.*

Singlet oxygen ($^1O_2$) is a weak oxidant that has strong electrophilicity and selectivity removes electrons from electron-rich substances.[1] Therefore, it is commonly used in the fields of green organic synthesis, photodynamic cancer treatment, and sewage purification.[2] Due to its long life, wide pH tolerance, and high selectivity, $^1O_2$ exhibits stronger resistance to environmental interference and higher selectivity of degradation than hydroxyl radicals ($^{\bullet}OH$) and sulfate radicals ($SO_4^{\bullet-}$), particularly in the field of wastewater treatment.[3] Currently, the disproportionation of superoxide radical ($O_2^{\bullet-}$), which is produced from the catalytic activation of H_2O_2, to produce $^1O_2$ is the most commonly used method.[4] Unfortunately, the Haber-Weiss reaction ($O_2^{\bullet-} + H_2O_2 \rightarrow {}^{\bullet}OH + OH^- + O_2$) significantly reduces the yield of $^1O_2$.[5] To avoid this competitive reaction, peroxymonosulfate (PMS) or peroxydisulfate (PDS) have been used to generate $^1O_2$ via self-decay, nucleophilic addition, and catalytic activation.[6] However, the formation of $^1O_2$ is generally accompanied by the generation of free radicals such as $^{\bullet}OH$ and $SO_4^{\bullet-}$.[7] And even the $^1O_2$ is only a secondary active species.[8] Therefore, there is an urgent need to develop new catalysts for highly selective and efficient generation of $^1O_2$.

Single-atom catalysts (SACs), which showed higher selectivity and efficiency in catalytic reactions than those of traditional catalysts, have been used to activate PMS for the generate of $^1O_2$.[9] And N-doped carbon supported SACs have exhibited significantly enhanced $^1O_2$ generation selectivity from the activated PMS. However, the mechanism of enhancement by different SACs vary, indicating that the metal atoms affects the selectivity of $^1O_2$.[10] Recently, theoretically constructed CoN_{2+2} SACs achieved a selectivity higher than 98 % for the generation of $^1O_2$ by activating PMS, which proved that the coordination atoms also play an important role in the selective generation of $^1O_2$.[11] The various types of N atoms present in the supports of SACs alter the different adsorption and activation mechanisms of PMS. Consequently, the generation of $^{\bullet}OH$, $SO_4^{\bullet-}$, and other radicals have not been eliminated to date.[12] Furthermore, the sparse doping of N, which fixes the metal atoms by coordination, causes the low metal loading, which retards the generation of $^1O_2$.[13] Therefore, the SACs having uniformly structured supports and abundant active sites are required for the selective generation of $^1O_2$. Graphitic carbon nitride (CN) has specified C and N sites and high N content, resulting in abundant and uniform single atomic fixation sites.[14] Consequently, when CN is used as the support, the obtained SACs would exhibit highly uniform and densely loaded metal active sites that facilitate the highly efficient activation of PMS to generate $^1O_2$ with 100 % selectivity.

Herein, a CN supported Fe SAC (Fe_1/CN) having a loading of up to 11.2 wt % of Fe active sites was prepared via the supermolecule method. Aberration-corrected high-angle annular dark-field scanning transmission electron microscopy (AC-HAADF-STEM) and X-ray absorption spectroscopy (XAS) proved the single atom dispersion and highly uniform Fe-N_4 centers of the Fe atoms in Fe_1/CN. Qualitative and quantitative analyses of the active species verified that Fe_1/

[*] Dr. L. S. Zhang,[+] Dr. X. H. Jiang,[+] Z. A. Zhong, L. Tian, Q. Sun, Prof. J. P. Zou, Prof. S. L. Luo
Key Laboratory of Jiangxi Province for Persistent Pollutants Control and Resources Recycle, Nanchang Hangkong University
Nanchang, Jiangxi 330063 (P. R. China)
E-mail: zjp_112@126.com
Prof. Y. T. Cui
SANKA High Technology Co. Ltd. 90-1
Kurimachi, Shingu-machi, Tatsuno, Hyogo 679-5155 (Japan)
Prof. X. Lu
State Key Laboratory of Physical Chemistry of Solid Surface, Xiamen University
Xiamen, Fujian 361005 (P. R. China)
[+] These authors contributed equally to this work.
Supporting information and the ORCID identification number(s) for the author(s) of this article can be found under: https://doi.org/10.1002/anie.202109488.

CN efficiently activated PMS to generate $^1O_2$ with 100% selectivity, which exceeds that of CN supported Fe nanoparticles (Fe_{NP}/CN), Co SAC (Co_1/CN), and Ni SAC (Ni_1/CN) catalysts. The high efficiency and selective generation of $^1O_2$ from Fe_1/CN activated PMS rapidly degraded p-chlorophenol (4-CP), and the optimized apparent rate constants (K_{obs}) were as high as 1.43 min^{-1} [Eq. (S1), Supporting Information]. Compared with Co and Ni sites, the density functional theory (DFT) calculations results demonstrated that the Fe sites in Fe_1/CN tend to adsorb the terminal O of PMS, which can facilitate the oxidization of PMS to form $SO_5^{\bullet-}$, and thereafter efficiently generated $^1O_2$ with 100% selectivity. Because it solely produced $^1O_2$, the Fe_1/CN activated PMS system exhibited strong resistance to interference from anions, cations, and natural organic matter (NOM), and had a wide pH tolerance and good cycle stability. This research opens up a new avenue for the efficient activation of PMS and 100% selective production of $^1O_2$.

The Fe_1/CN was synthesized by the supermolecule method reported in our previous work with slight modification.[15] X-ray diffraction (XRD) patterns and Fourier-transform infrared (FT-IR) spectra exhibited the CN matrix of Fe_1/CN (Figure S1, Supporting Information).[16] No characteristic peaks associated with Fe compounds were observed in Fe_1/CN.[17] As shown in Figure 1 a and b, atomic force microscopy (AFM) and transmission electron microscopy (TEM) images captured the lamellar structure of Fe_1/CN, which had a thickness of approximately 4 nm, and did not contain Fe nanoparticles. Furthermore, AC-HAADF-STEM and energy-dispersive X-ray (EDX) images demonstrated that all the Fe atoms (the bright spots highlighted by orange circles) were atomically dispersed on the CN support (Figure 1 c and d).

As shown in Figure 1 e, the absorption edge of Fe_1/CN was located between those of FeO and Fe_2O_3 in the Fe K-edge X-ray absorption near-edge structure (XANES) spectra, indicating the oxidation state of the Fe atom in Fe_1/CN ($Fe^{\delta+}$, $2 < \delta < 3$).[18] The Fourier-transform extended X-ray absorption fine structure (FT-EXAFS) spectrum (Figure 1 f) of Fe_1/CN exhibits a solitary peak at approximately 1.7 Å, which is attributed to the Fe–N bond. In comparison to Fe foil, FeO, and Fe_2O_3, no Fe-Fe or Fe-O peaks were observed, indicating the absence of Fe clusters or oxides in Fe_1/CN. In the wavelet transform (WT) contour plots (Figure S2), the intensity maxima of Fe foil at 7.9 $Å^{-1}$ is attributed to Fe–Fe bonds.[19] In addition, a solitary intensity maximum of Fe_1/CN at 4.2 $Å^{-1}$ can be ascribed to the Fe–N bond.[20] The EXAFS-fitting results show that the coordination number of Fe is 4 (Table S1, Supporting Information). All the above results confirm that the Fe atoms in Fe_1/CN are atomically dispersed in a Fe-N_4 configuration (Figure 1 g).

The effect of Fe_1/CN activation on PMS was evaluated by the degradation of organic pollutants. As shown in Figures 2 a and S3, Fe_1/CN achieved the highest removal rate of 4-CP with a K_{obs} of 0.55 min^{-1}, which is 5.4, 1.7, and 6.5 times than that of Fe_{NP}/CN, Co_1/CN, and Ni_1/CN, respectively. Total organic carbon (TOC) test proved that the 4-CP was degraded into CO_2 and H_2O (Figure S4). In addition, other organic pollutants can also be rapidly degraded (Figure S5). Fe_1/CNs having different Fe loadings exhibited volcano-like plots of the degradation rates of 4-CP, with the maximum rate being obtained at the Fe content of 7.0 wt% (Figure S6). Furthermore, Fe_1/CNs having different surface concentrations of Fe atoms but similar total Fe contents were also used to degrade 4-CP (Figure S7 and Table S2).[21] As shown in Figure S8, the rate of degradation of 4-CP increased from 0.55 to 1.43 min^{-1} as the surface concentration of Fe atoms increased. When CNs or no catalyst was added, 4-CP was not removed in the PMS solution (Figure S9), indicating that the expedited degradation of Fe_1/CNs did not stem from the

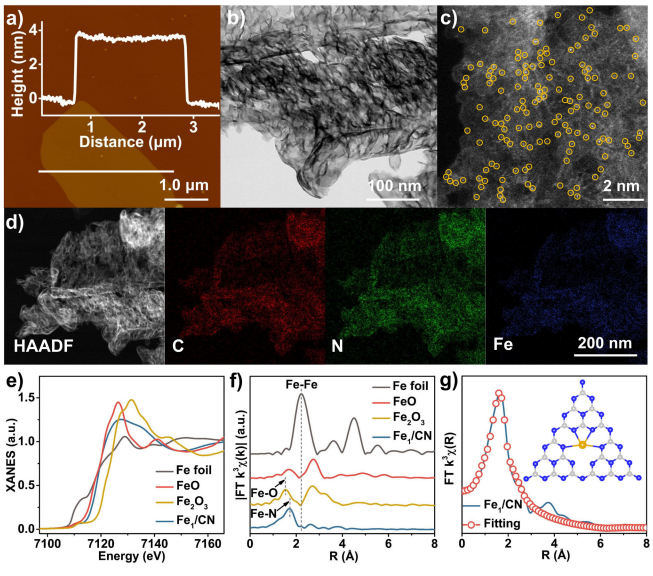

Figure 1. a) AFM and corresponding height profiles along the white line, b) TEM, c) AC-HAADF-STEM, and d) EDX images of the Fe_1/CN; e) normalized Fe K-edge XANES and f) k^3-weighted Fourier transform spectra of Fe foil, FeO, Fe_2O_3, and Fe_1/CN; and g) EXAFS fitting curve in R space (inset: structural model of Fe_1/CN, Fe: orange, N: blue, C: grey).

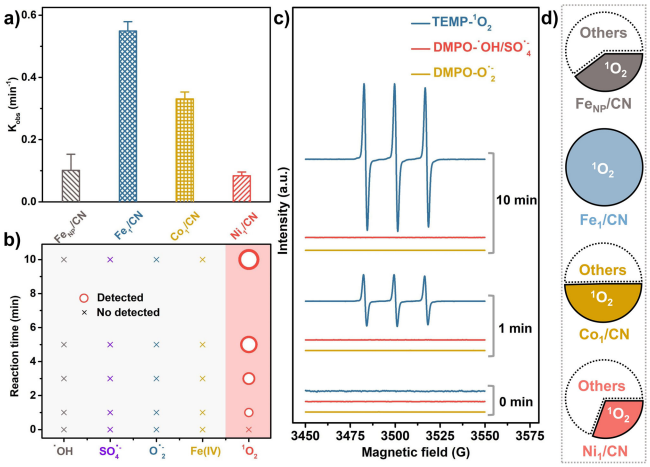

Figure 2. a) 4-CP degradation rate in different catalysts activated PMS systems; b) qualitative and quantitative analyses of active species present in Fe_1/CN activated PMS system; c) EPR spectra of •OH, $SO_4^{\bullet-}$, $O_2^{\bullet-}$, and $^1O_2$ in Fe_1/CN activated PMS systems; and d) the proportion of $^1O_2$ in different catalysts activated PMS systems.

enhanced surface area of CN. Therefore, the quicker degradation of Fe_1/CN was driven by the enhanced surface concentration of Fe atoms.

The effect of the state of the Fe species on PMS activation was studied as well. In the homogeneous Fe^{2+} activated PMS system, 4-CP was rapidly degraded in the first minute, however, its removal did not continue (Figure S10). Replenishing the Fe^{2+} content in the fifth minute permitted part of the remaining 4-CP to be degraded, indicating that Fe^{2+} is consumed during the activation of PMS.[22] Replacing Fe^{2+} using Fe^{3+} halted the degradation of 4-CP. We infer that PMS is reduced by the Fe^{2+} to generate radical active species and Fe^{3+}, and the generated Fe^{3+} cannot be restored to Fe^{2+} for further activation of PMS despite the presence of CN (Figure S11).[23] This indicate that the strong interaction between CN and Fe plays important roles in the continuous activation of PMS. Although homocatalysis is generally more rapid than that via heterocatalysis, the Fe_1/CN heterocatalyst degraded 4-CP more rapidly than the homogeneous Fe^{2+} in the PMS system did (Figure S12). In summary, Fe_1/CN combines the advantages of high efficiency (of homocatalysis) and sustainability (of heterocatalysis), achieving rapid and continuous activation of PMS for the degradation of organic pollutant.

As shown in Figures S4 and S13, the rate of consumption of PMS was more rapid than the degradation of 4-CP in the Fe_1/CN activated PMS system, indicating that the active species can be rapidly and abundantly produced in the system. Nonetheless, active species such as $SO_4^{\bullet-}$, $^{\bullet}OH$, $O_2^{\bullet-}$, and high valent iron (Fe^{IV}) were not detected during the reaction (Figure 2b). Specifically, the absorption intensity of nitro blue tetrazolium (NBT) at 259 nm (the probe for $O_2^{\bullet-}$) and the photoluminescence (PL) intensity of 2-hydroxy terephthalic (TA-OH) at 425 nm (the probe for $^{\bullet}OH$) remained constant throughout the reaction (Figure S14).[24] Furthermore, when the hydroxybenzoic acid (HBA) and methyl phenyl sulfoxide (PMSO) were used to probe for $SO_4^{\bullet-}$ and Fe^{IV}, respectively, no singles corresponding to p-benzoquinone (BQ) and methyl phenyl sulfone ($PMSO_2$) were recorded at the retention times of 5.0 and 9.5 min during the reaction (Figure S15).[25] Furthermore, the scavengers of MeOH, EtOH, KI, BQ, isopropanol (IPA), tert-butanol (TBA), superoxide dismutase (SOD), and catalase (CAT) did not influence the degradation rate of 4-CP (Figure S16), implying the absence of $SO_4^{\bullet-}$, $^{\bullet}OH$, and $O_2^{\bullet-}$ active species. In addition, atrazine (ATZ) and PMSO were not degraded by the Fe_1/CN activated PMS system (Figure S17), indicating the absence of $^{\bullet}OH$ and Fe^{IV}.[6a] When 5,5-dimethyl-1-pyrroline-N-oxide (DMPO) and 2,2,6,6-tetramethyl-4-piperidinyloxyl (TEMP) were employed to capture the $SO_4^{\bullet-}$, $^{\bullet}OH$, $O_2^{\bullet-}$, and $^1O_2$, respectively, no electron paramagnetic resonance (EPR) characteristic signals of DMPO-$SO_4^{\bullet-}$, DMPO-$^{\bullet}OH$, and DMPO-$O_2^{\bullet-}$ was recorded during the reaction (Figure 2c).[26] Relatively, three characteristic peaks of TEMP-$^1O_2$ were clearly detected in the EPR spectrum, and the signal intensity continually increased during the reaction, indicating that Fe_1/CN can continuously activate PMS to form $^1O_2$.[4b] When L-histidine, furfuryl alcohol (FFA), or NaN_3 was added, the degradation rate of 4-CP was sharply decreased, and the inhibitory effect increases with increase in the dosage of the scavengers (Figure S18), suggesting that $^1O_2$ is the sole active species. In addition, $^1O_2$ remained the sole active species regardless of the loading amount and surface exposure ratio of the Fe single-atoms in Fe_1/CNs (Figure S19). However, the $SO_4^{\bullet-}$, $^{\bullet}OH$, $^1O_2$, and $O_2^{\bullet-}$ active species were all detected in the Fe_{NP}/CNs activated PMS systems (Figure S20), in line with the trapping tests (Figure S21). With the decrease of Fe sizes from 200 nm to single-atom, the generated proportion of $^1O_2$ increased from 43% to 100% [Figures 2d, S22, and S23, Eq. (S2)–(S6)].[27] In comparison, the selectivities of Co_1/CN and Ni_1/CN, which were also SACs, for generating $^1O_2$ by activating PMS were approximately 49% and 27%, respectively (Figures 2d and S24). Hence, Fe_1/CN activated PMS system produces solely $^1O_2$, whereas Fe_{NP}/CN, Co_1/CN, and Ni_1/CN also produce the $SO_4^{\bullet-}$, $^{\bullet}OH$, $^1O_2$, and $O_2^{\bullet-}$ active species.

As shown in Figure 3a, the atmospheres (Ar, O_2, or air) did not influence the degradation rate of 4-CP, suggesting that the O for $^1O_2$ was not derived from dissolved oxygen. As shown in Figures 3b and S16, the EPR singles strength of $^1O_2$ continue to increase and the degradation rate of 4-CP had no change in the present of BQ, indicating that $^1O_2$ was not generated from $O_2^{\bullet-}$. The aforementioned results indicate that Fe_1/CN can efficiently activate PMS to directly generate $^1O_2$ while avoiding the Haber-Weiss competitive reaction.[12c] In linear sweep voltammetry (LSV) analyses (Figure 3c), the current density of the Fe_1/CN electrode significantly increased in the presence of PMS, which confirms that electrons transfer from PMS to the Fe single-atoms.[11] As shown in Figure 3d and Table S3, the pyridine nitrogen (pyr-N) site of Co_1/CN adsorbed the O2 site of PMS and the graphitic nitrogen (gra-N) site of Ni_1/CN adsorbed the O1 site of PMS, which promoted the reduction of PMS to generate $SO_4^{\bullet-}$ and $^{\bullet}OH$. In addition, Fe nanoparticles in Fe_{NP}/CN preferentially adsorbed the O2 site of PMS, which promoted the decomposition of PMS into $SO_4^{\bullet-}$ and $^{\bullet}OH$ via a com-

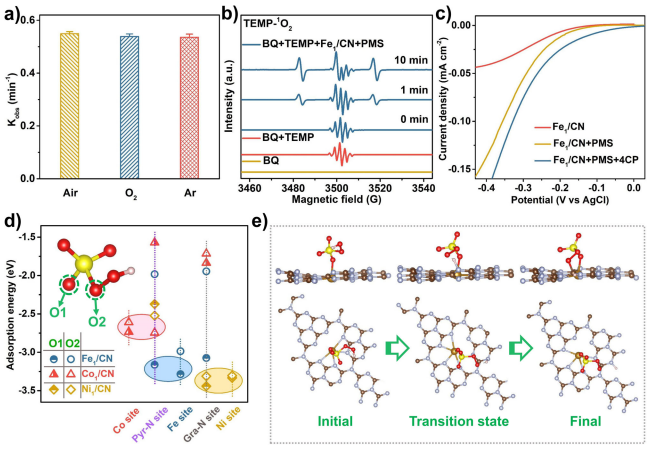

Figure 3. a) Degradation rate of 4-CP by Fe_1/CN activated PMS under different atmospheres; b) EPR spectra for the detection of $^1O_2$ in the presence of TEMP and BQ using water as the solvent; c) LSV curves of Fe_1/CN under different conditions; d) the adsorption energies of PMS onto the different sites of catalysts (inset: molecular model of PMS); e) evolution process of PMS into $SO_5^{\bullet-}$ on Fe_1/CN.

pletely spontaneous process.[28] In contrast, Fe_1/CN tends to adsorb the O1 site of PMS on the Fe site, which promoted the oxidation of PMS to $SO_5^{\bullet-}$ by the loss of the H atom (Figure 3e). Due to the high reaction rate ($\approx 2\times10^8\ M^{-1}s^{-1}$) and low activation energy (7.4 ± 2.4 kcal mol^{-1}), $SO_5^{\bullet-}$ rapidly self-reaction to generate $S_2O_8^{2-}$, $SO_4^{\bullet-}$, and $^1O_2$ [Figure 3e and Eq. (1)–(3)].

$$HSO_5^- \rightarrow SO_5^{\bullet-} + H^+ + e^- \quad (1)$$

$$SO_5^{\bullet-} + SO_5^{\bullet-} \rightarrow S_2O_8^{2-} + {}^1O_2 \quad (2)$$

$$SO_5^{\bullet-} + SO_5^{\bullet-} \rightarrow 2\,SO_4^{2-} + {}^1O_2 \quad (3)$$

As shown in Figures 4a,b, and S25, all of the anions (F^-, Cl^-, HCO_3^-, and SO_3^{2-}), cations (Na^+, K^+, Mg^{2+}, and Ca^{2+}), and NOM did not significantly influence the degradation rate of 4-CP at any of the dosages tested. This indicates that the Fe_1/CN activated PMS undergoes less interference from common background organic and inorganic substances present in water.[29] Moreover, Fe_1/CN could activate PMS for the degradation of 4-CP effectively in the pH range of 3.4–10.8 (Figure 4c), which verifies that Fe_1/CN catalyst and $^1O_2$ active species have strong tolerance to the pH of the solution. In contrast, the rate of degradation of 4-CP changed significantly when diverse anions, cations, and NOM were introduced into the Fe_{NP}/CN activated PMS system (Figures 4b and S26), which shows that the degradation process of 4-CP with $SO_4^{\bullet-}$ and $^{\bullet}OH$ radicals is easily disturbed by the environmental substances.[30] More importantly, Fe_1/CN achieved similar rates of degradation of 4-CP in natural (tap water, the Poyang Lake water, and the Yangtze River water) and deionized waters (Figure 4d), indicating its excellent practical application prospects. As shown in Figure S27, the cyclic tests demonstrated that Fe_1/CN is more stable than Fe_{NP}/CN during the activation of PMS for the degradation of 4-CP. In summary, the Fe_1/CN activated PMS system exhibited excellent pH adaptability, inorganic ions, and NOM interference tolerance, and stability.

This work prepared Fe_1/CN catalysts having a highly uniform Fe-N_4 structure using the supermolecule method. When Fe_1/CN was used to activate PMS, $^1O_2$ active species was generated at 100% selectivity, which facilitated an extremely rapid 4-CP degradation rate of 1.43 min^{-1}. DFT calculations showed that the Fe-N_4 sites can adsorb the terminal O of PMS and then oxidized to $SO_5^{\bullet-}$, and subsequently generate $^1O_2$. Due to the generation of $^1O_2$ with 100% selectivity, the Fe_1/CN activated PMS system exhibits strong resistance to interference from environmental media containing anions, cations, and NOM, and operates efficiently in the wide pH range of 3–11. Furthermore, the cycle tests and nature water degradation of 4-CP verify the excellent stability and practical application prospect of Fe_1/CN. This work provides a new idea for selectively producing $^1O_2$, which can achieve highly selective degradation of pollutants in wastewater.

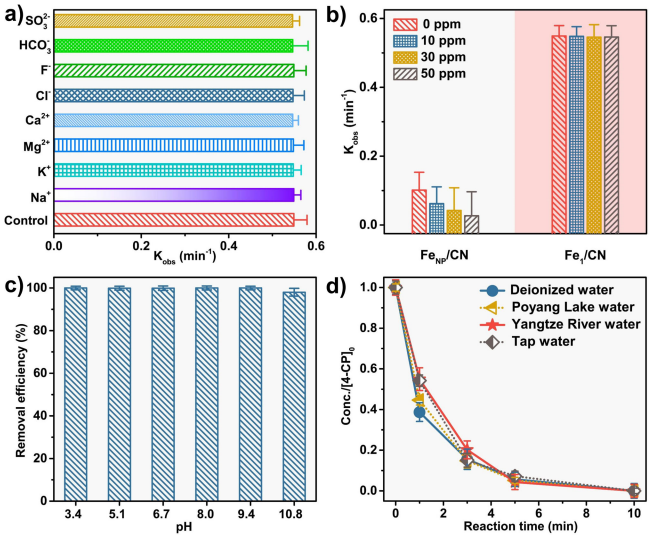

Figure 4. 4-CP degradation rate in a) Fe_1/CN activated PMS system in the presence of different ions; b) Fe_1/CN and Fe_{NP}/CN activated PMS systems at different NOM concentrations; c) removal efficiency of 4-CP at different initial pH; and d) the 4-CP degradation rate in different natural waters of Fe_1/CN activated PMS systems.

Acknowledgements

We gratefully acknowledge the financial support of the National Natural Science Foundation of China (51868050, 52100186, 52170082, 51938007, 51720105001, and 51878325) and the Natural Science Foundation of Jiangxi Province (20202BAB213011). The synchrotron radiation experiment for XAFS was performed at the BL14B1 of Japan Atomic Energy Agency with the approval of JAEA and Japan Synchrotron Radiation Research Institute (Proposal Nos. 2016B3618, 2018A3631).

Conflict of Interest

The authors declare no conflict of interest.

Keywords: degradation · Fe single-atom catalyst · graphitic carbon nitride · organic pollutants · singlet oxygen

[1] a) A. A. Ghogare, A. Greer, *Chem. Rev.* **2016**, *116*, 9994–10034; b) Z. J. Zhou, J. B. Song, R. Tian, Z. Yang, G. C. Yu, L. S. Lin, G. F. Zhang, W. P. Fan, F. W. Zhang, G. Niu, L. M. Nie, X. Y. Chen, *Angew. Chem. Int. Ed.* **2017**, *56*, 6492–6496; *Angew. Chem.* **2017**, *129*, 6592–6596; c) F. Ramel, S. Birtic, C. Ginies, L. Soubigou-Taconnat, C. Triantaphylidès, M. Havaux, *Proc. Natl. Acad. Sci. USA* **2012**, *109*, 5535–5540.

[2] a) S. S. He, S. Y. Lu, S. Liu, T. R. Li, J. L. Li, S. H. Sun, M. L. Liu, K. Liang, X. Fu, F. J. Chen, G. P. Meng, L. Zhang, J. Hai, B. D. Wang, *Chem. Sci.* **2020**, *11*, 8817–8827; b) H. B. Cheng, B. Qiao, H. Li, J. Cao, Y. L. Luo, K. M. K. Swamy, J. Zhao, Z. G. Wang, J. Y. Lee, X. J. Liang, J. Yoon, *J. Am. Chem. Soc.* **2021**, *143*, 2413–2422; c) Y. M. Zhao, M. Sun, X. X. Wang, C. Wang, D. W. Lu, W. Ma, S. A. Kube, J. Ma, M. Elimelech, *Nat. Commun.* **2020**, *11*, 6228.

[3] a) N. Zhao, K. Y. Liu, C. He, J. Cao, W. H. Zhang, T. J. Zhao, D. C. W. Tsang, R. L. Qiu, *Environ. Int.* **2020**, *143*, 105899;

b) Y. G. Bu, H. C. Li, W. J. Yu, Y. F. Pan, L. J. Li, Y. F. Wang, L. T. Pu, J. Ding, G. D. Gao, B. C. Pan, *Environ. Sci. Technol.* **2021**, *55*, 2110 – 2120; c) T. Y. Li, L. F. Ge, X. X. Peng, W. Wang, W. X. Zhang, *Water Res.* **2021**, *190*, 116777.

[4] a) W. J. Duan, J. L. He, Z. L. Wei, Z. R. Dai, C. H. Feng, *Environ. Sci. Nano* **2020**, *7*, 2982 – 2994; b) Z. C. Yang, J. S. Qian, A. Q. Yu, B. C. Pan, *Proc. Natl. Acad. Sci. USA* **2019**, *116*, 6659 – 6664; c) J. H. Li, Q. Y. Yan, P. C. Yin, S. Y. Mine, M. Matsuoka, M. Y. Xing, *Angew. Chem. Int. Ed.* **2021**, *60*, 2903 – 2908; *Angew. Chem.* **2021**, *133*, 2939 – 2944; d) Q. Y. Yan, C. Lian, K. Huang, L. H. Liang, H. R. Yu, P. C. Yin, J. L. Zhang, M. Y. Xing, *Angew. Chem. Int. Ed.* **2021**, *60*, 17155 – 17163; *Angew. Chem.* **2021**, *133*, 17292 – 17300.

[5] a) X. T. Li, J. Wang, X. G. Duan, Y. Li, X. B. Fan, G. L. Zhang, F. B. Zhang, W. C. Peng, *ACS Catal.* **2021**, *11*, 4848 – 4861; b) Q. Y. Yi, J. H. Ji, B. Shen, C. C. Dong, J. Liu, J. L. Zhang, M. Y. Xing, *Environ. Sci. Technol.* **2019**, *53*, 9725 – 9733.

[6] a) P. H. Shao, J. Y. Tian, F. Yang, X. G. Duan, S. S. Gao, W. X. Shi, X. B. Luo, F. Y. Cui, S. L. Luo, S. B. Wang, *Adv. Funct. Mater.* **2018**, *28*, 1705295; b) Y. Zhou, J. Jiang, Y. Gao, S. Y. Pang, Y. Yang, J. Ma, J. Gu, J. Li, Z. Wang, L. H. Wang, L. P. Yuan, Y. Yang, *Water Res.* **2017**, *125*, 209 – 218; c) Y. N. Liu, J. Luo, L. Tang, C. Y. Feng, J. J. Wang, Y. C. Deng, H. Y. Liu, J. F. Yu, H. P. Feng, J. J. Wang, *ACS Catal.* **2020**, *10*, 14857 – 14870.

[7] a) J. Q. Li, M. T. Li, H. Q. Sun, Z. M. Ao, S. B. Wang, S. M. Liu, *ACS Catal.* **2020**, *10*, 3516 – 3525; b) B. J. Sun, W. J. Ma, N. Wang, P. Xu, L. J. Zhang, B. N. Wang, H. H. Zhao, K. Y. A. Lin, Y. C. Du, *Environ. Sci. Technol.* **2019**, *53*, 9771 – 9780; c) Z. Liu, H. J. Ding, C. Zhao, T. Wang, P. Wang, D. D. Dioysiou, *Water Res.* **2019**, *159*, 111 – 121.

[8] a) Y. Yang, G. Banerjee, G. W. Brudvig, J. H. Kim, J. J. Pignatello, *Environ. Sci. Technol.* **2018**, *52*, 5911 – 5919; b) S. Z. Wang, Y. Liu, J. L. Wang, *Environ. Sci. Technol.* **2020**, *54*, 10361 – 10369.

[9] a) T. Ouyang, A. N. Chen, Z. Z. He, Z. Q. Liu, Y. X. Tong, *Chem. Commun.* **2018**, *54*, 9901 – 9904; b) H. F. Qi, J. Yang, F. Liu, L. L. Zhang, J. Y. Yang, X. Y. Liu, L. Li, Y. Su, Y. F. Liu, R. Hao, A. Q. Wang, T. Zhang, *Nat. Commun.* **2021**, *12*, 3295; c) Y. F. Zhao, H. Zhou, X. R. Zhu, Y. T. Qu, C. Xiong, Z. G. Xue, Q. W. Zhang, X. K. Liu, F. Y. Zhou, X. M. Mou, W. Y. Wang, M. Chen, Y. Xiong, X. G. Lin, Y. Lin, W. X. Chen, H. J. Wang, Z. Jiang, L. R. Zheng, T. Yao, J. C. Dong, S. Q. Wei, W. X. Huang, L. Gu, J. Luo, Y. F. Li, Y. E. Wu, *Nat. Catal.* **2021**, *4*, 134 – 143.

[10] a) X. N. Li, X. Huang, S. B. Xi, S. Miao, J. Ding, W. Z. Cai, S. Liu, X. L. Yang, H. B. Yang, J. J. Gao, J. H. Wang, Y. Q. Huang, T. Zhang, B. Liu, *J. Am. Chem. Soc.* **2018**, *140*, 12469 – 12475; b) S. J. Zuo, X. M. Jin, X. W. Wang, Y. H. Lu, Q. Zhu, J. W. Wang, W. P. Liu, Y. H. Du, J. Wang, *Appl. Catal. B* **2021**, *282*, 119551.

[11] X. Y. Mi, P. F. Wang, S. Z. Xu, L. N. Su, H. Zhong, H. T. Wang, Y. Li, S. H. Zhan, *Angew. Chem. Int. Ed.* **2021**, *60*, 4588 – 4593; *Angew. Chem.* **2021**, *133*, 4638 – 4643.

[12] a) C. H. Chu, J. Yang, X. C. Zhou, D. H. Huang, H. F. Qi, S. Weon, J. F. Li, M. Elimelech, A. Q. Wang, J. H. Kim, *Environ. Sci. Technol.* **2021**, *55*, 1242 – 1250; b) Y. F. Qi, J. Li, Y. Q. Zhang, Q. Cao, Y. M. Si, Z. R. Wu, M. Akram, X. Xu, *Appl. Catal. B* **2021**, *286*, 119910; c) Y. W. Gao, Y. Zhu, T. Li, Z. H. Chen, Q. K. Jiang, Z. Y. Zhao, X. Y. Liang, C. Hu, *Environ. Sci. Technol.* **2021**, *55*, 8318 – 8328.

[13] a) N. J. Du, Y. Liu, Q. J. Li, W. Miao, D. D. Wang, S. Mao, *Chem. Eng. J.* **2021**, *413*, 127545; b) Y. Xiong, W. M. Sun, P. Y. Xin, W. X. Chen, X. S. Zheng, W. S. Yan, L. R. Zheng, J. C. Dong, J. Zhang, D. S. Wang, Y. D. Li, *Adv. Mater.* **2020**, *32*, 2000896; c) L. Jiao, R. Zhang, G. Wan, W. J. Yang, X. Wan, H. Zhou, J. L. Shui, S. H. Yu, H. L. Jiang, *Nat. Commun.* **2020**, *11*, 2831.

[14] a) P. Chen, B. Lei, X. A. Dong, H. Wang, J. P. Sheng, W. Cui, J. Y. Li, Y. J. Sun, Z. M. Wang, F. Dong, *ACS Nano* **2020**, *14*, 15841 – 15852; b) Y. Li, B. H. Li, D. N. Zhang, L. Lei, Q. J. Xiang, *ACS Nano* **2020**, *14*, 10552 – 10561; c) Z. Y. Teng, Q. T. Zhang, H. B. Yang, K. Kato, W. J. Yang, Y. R. Lu, S. X. Liu, C. Y. Wang, A. Yamakata, C. L. Su, B. Liu, T. Ohno, *Nat. Catal.* **2021**, *4*, 374 – 384.

[15] X. H. Jiang, L. S. Zhang, H. Y. Liu, D. S. Wu, F. Y. Wu, L. Tian, L. L. Liu, J. P. Zou, S. L. Luo, B. B. Chen, *Angew. Chem. Int. Ed.* **2020**, *59*, 23112 – 23116; *Angew. Chem.* **2020**, *132*, 23312 – 23316.

[16] J. W. Xu, X. L. Zheng, Z. P. Feng, Z. Y. Lu, Z. W. Zhang, W. Huang, Y. B. Li, D. Vuckovic, Y. Q. Li, S. Dai, G. X. Chen, K. C. Wang, H. S. Wang, J. K. Chen, W. Mitch, Y. Cui, *Nat. Sustainability* **2021**, *4*, 233 – 241.

[17] J. W. Zheng, K. Lebedev, S. Wu, C. Huang, T. Ayvali, T. S. Wu, Y. Y. Li, P. L. Ho, L. Y. Soo, A. Kirkland, S. C. E. Tsang, *J. Am. Chem. Soc.* **2021**, *143*, 7979 – 7990.

[18] Y. F. Zhu, S. F. Yuk, J. Zheng, M. T. Nguyen, M. S. Lee, J. Szanyi, L. Kovarik, Z. H. Zhu, M. Balasubramanian, V. A. Glezakou, J. L. Fulton, J. A. Lercher, R. Y. Rousseau, O. Y. Gutiérrez, *J. Am. Chem. Soc.* **2021**, *143*, 5540 – 5549.

[19] X. D. Long, Z. L. Li, G. Gao, P. Sun, J. Wang, B. S. Zhang, J. Zhong, Z. Jiang, F. W. Li, *Nat. Commun.* **2020**, *11*, 4074.

[20] Y. X. Li, S. Y. Wang, X. S. Wang, Y. He, Q. Wang, Y. B. Li, M. L. Li, G. L. Yang, J. D. Yi, H. W. Lin, D. K. Huang, L. Li, H. Chen, J. H. Ye, *J. Am. Chem. Soc.* **2020**, *142*, 19259 – 19267.

[21] X. D. Jia, Y. F. Zhao, G. B. Chen, L. Shang, R. Shi, X. F. Kang, G. I. N. Waterhouse, L. Z. Wu, C. H. Tung, T. R. Zhang, *Adv. Energy Mater.* **2016**, *6*, 1502585.

[22] P. Zhou, W. Ren, G. Nie, X. J. Li, X. G. Duan, Y. L. Zhang, S. B. Wang, *Angew. Chem. Int. Ed.* **2020**, *59*, 16517 – 16526; *Angew. Chem.* **2020**, *132*, 16660 – 16669.

[23] a) M. Y. Xing, W. J. Xu, C. C. Dong, Y. C. Bai, J. B. Zeng, Y. Zhou, J. L. Zhang, Y. D. Yin, *Chem* **2018**, *4*, 1359 – 1372; b) Z. L. Wei, H. L. Xu, Z. C. Lei, X. Y. Yi, C. H. Feng, Z. Dang, *Chin. Chem. Lett.* **2021**, https://doi.org/10.1016/j.cclet.2021.07.006.

[24] H. Li, H. Shang, Y. H. Li, X. M. Cao, Z. P. Yang, Z. H. Ai, L. Z. Zhang, *Environ. Sci. Technol.* **2019**, *53*, 6964 – 6971.

[25] H. Y. Zhou, J. L. Peng, J. Y. Li, J. J. You, L. D. Lai, R. Liu, Z. M. Ao, G. Yao, B. Lai, *Water Res.* **2021**, *188*, 116529.

[26] L. P. Wu, B. Li, Y. Li, X. B. Fan, F. B. Zhang, G. L. Zhang, Q. Xia, W. C. Peng, *ACS Catal.* **2021**, *11*, 5532 – 5543.

[27] X. Q. Zhou, M. Y. Luo, C. Y. Xie, H. B. Wang, J. Wang, Z. L. Chen, J. W. Xiao, Z. Q. Chen, *Appl. Catal. B* **2021**, *282*, 119605.

[28] Z. L. Wu, Y. P. Wang, Z. K. Xiong, Z. M. Ao, S. Y. Pu, G. Yao, B. Lai, *Appl. Catal. B* **2020**, *277*, 119136.

[29] S. Q. Wu, X. Hua, B. W. Ma, H. W. Fan, R. Miao, M. Ulbricht, C. Z. Hu, *Environ. Sci. Technol.* **2021**, *55*, 5442 – 5452.

[30] K. Qian, H. Chen, W. L. Li, Z. M. Ao, Y. N. Wu, X. H. Guan, *Environ. Sci. Technol.* **2021**, *55*, 7034 – 7043.

Manuscript received: July 15, 2021
Accepted manuscript online: August 3, 2021
Version of record online: August 31, 2021

